Cyclic Voltammetry to Study Dynamics of Ion Insertion in Porous Materials

Cyrille Costentin

ADVANCED ENERGY & SUSTAINABILITY RESEARCH
Open Access
www.advenergysustres.com

Cyclic Voltammetry to Study Dynamics of Ion Insertion in Porous Materials

Cyrille Costentin

Electrochemical charge storage in porous materials is associated with ion adsorption at the meso/nanopores surface (physical insertion) and/or insertion in the bulk material (chemical insertion). The first process is capacitive whereas the second is Faradaic. A model is brought about for describing the cyclic voltammetry responses of these systems and their dependence upon the various intrinsic and operational governing parameters. These responses may be considered as illustrating the behaviors expected in working conditions in terms of diagnosis of the main phenomena at work and of their mutual interactions, namely, dynamics of double-layer charging, transport in solution, transport in the pores, interfacial transfer kinetics, and transport in the material bulk. Several limiting cases are examined in details and discussed, focusing on the effect of scan rate as a widely used diagnostic tool.

1. Introduction

The current large demand for energy storage makes the development of batteries and double-layer charging devices an active contemporary research area. New meso- or nanostructured electrode systems are almost daily proposed, thus calling for efforts to identify the phenomena at work and analyze their performances. Analytical methods offer the opportunity for a rapid screening of the electrochemical behavior of interesting new material for energy storage. Among these methods, cyclic voltammetry (CV) is one of the most popular. It consists of applying to a working electrode of small dimensions (disk of mm s diameters) a triangular potential while recording the ensuing current. This working electrode is part of a three-electrode setup, which allows, by means of a potentiostat, the precise definition of its potential versus a reference electrode, while the current flows through the counter electrode. The electrodes are immersed in a solution containing a concentrated electrolyte, which minimizes, albeit not suppresses, Ohmic drop within the mesostructure and in the bathing solution as discussed in the following sections. The advantage of CV is that the timescale of the experiment can be easily changed by varying the rate at which the working electrode potential is scanned. Herein, we discuss the application of CV to the investigation of electrochemical energy storage systems, either characterized by a double-layer charging response, or a Faradaic response, or both. Systems of practical interest do not involve a planar disk working electrode but rather a composite electrode tens of micrometers in thickness containing the material, activated carbon, and binder, flooded with electrolyte and having meso- and nanostructures. Their behavior in CV is considered as representative of the main phenomena at work in real conditions.

There are many reviews in the literature on the modeling of porous materials for energy storage[1] but we focus here on the use of CV to characterize ion insertion during charge storage in porous material. In that endeavor, CV analysis may involve a discouragingly large number of factors preventing the establishment of diagnostic criteria and derivation values of the pertinent governing parameters.[1e] This situation can be improved in two ways. The first is to recourse to dimensionless parameters that allow grouping together several operational factors. The second is a reasonable simplification of the starting assumptions that would however uphold the mechanistic ingredients that ensure the analysis to handle most cases of practical interest. This strategy is illustrated in the following by application of these simplified approaches to emblematic experimental examples.

We discuss successively the capacitive and Faradaic components of the CV response considering situations where both components can be separated due to the presence of a blocking electrolyte or a large concentration of the inserting ion in the electrolyte.

2. Results and Discussion

The electrodes considered here are porous solid materials penetrated by the solvent and the electrolyte present in the bathing solution. Ions are able to insert in the porous structure upon variation of the electrode potential. The solid part of the electrode is an electronic conductor in contact with the base electrode onto which the porous material is deposited.[2] This may be the case only in a restricted range of potential if we are dealing with a

C. Costentin
DCM
Université Grenoble Alpes, CNRS
Grenoble 38000, France
E-mail: cyrille.costentin@univ-grenoble-alpes.fr

The ORCID identification number(s) for the author(s) of this article can be found under https://doi.org/10.1002/aesr.202300242.

DOI: 10.1002/aesr.202300242

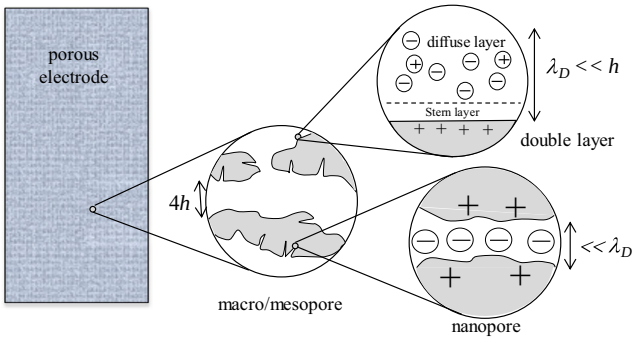

Figure 1. Schematic view of a porous insertion electrode. 4*h*: average size of mesopores. λ_D: Debye screening distance. Adapted with permission.[4] Copyright 2019, American Chemical Society.

semiconductor such as metal oxide electrodeposited films.[3] Macropores (size > 50 nm), mesopores (2–50 nm), and nanopores (size: few nm) are filled with the electrolyte (**Figure 1**).

Insertion of ions into these pores is referred to as *physical insertion* in the electrode as it is driven by a capacitive process, that is, corresponds to accumulation of charge at the electrolyte/solid interface upon polarization of the solid (vs. the solution) as shown in Figure 1.[4] It is worth making a distinction between ion physical insertion in the pores (including nanosized pores as shown in Figure 1) and ion insertion into the solid conductive material (chemical insertion) as summarized in **Figure 2**.

The density of nanopores may be very large with porous carbon materials, giving rise to what is usually named "supercapacitors".[5] This is also what happens with amorphous electrodeposited metal oxides made of nanoparticles or of stacked nanocrystallites,[6] hence leading to very large volumic capacitances. In the potential range where they are used for energy storage, these systems are of capacitive nature.[7,8] It is the result of a preliminary Faradaic oxidation, which changes the initial insulator nature of the oxide material into that of an electric conductor. This true capacitive behavior contrasts the popular but unclear notion of "pseudocapacitance" that has long prevailed to qualify these materials.[9] Similar behaviors are observed with flaky structured material such as MXenes.[10]

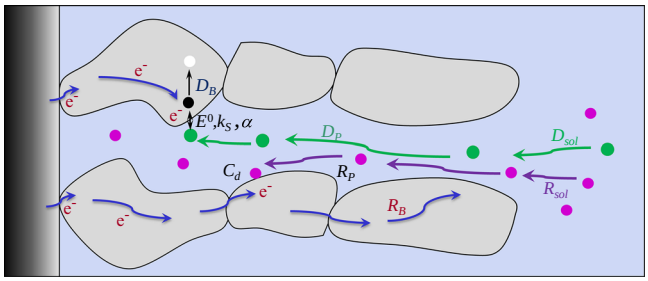

Figure 2. Schematic representation of the main phenomena taking place upon charge storage in a porous material: diffusion of the inserting ion in solution (D_{sol}), in the pores (D_P), in the solid conductive material (D_B); resistance of the solution (R_{sol}), of the pores (R_P), of the material (R_B); double-layer charging capacitance (C_d); interfacial charge transfer (E^0, k_S, α).

Examples of capacitive CV responses observed with these three types of materials are shown in **Figure 3**. The term of ion "intercalation" is more commonly used than ion insertion in the case of flaky structures such as those in MXenes matching the idea that the ions get into the space in between two flake planes. In sake of generality, we go on with the "insertion" terminology.

While physical insertion refers to double-layer capacitive charging, chemical insertion is a Faradaic process. Indeed, charged particles—here the inserting ions—are crossing the solid/electrolyte interface through a potential difference defined by the value of the electrode potential at the corresponding position in the porous electrode. The process is thermodynamically characterized by a standard potential corresponding to localization of electrons and ions at defined positions in the conductive structure, noting that many of these redox sites may be sited at the surface of the solid. We view the transport of ions in the solid structure as occurring through a series of electron coupled/ion self-exchange processes between redox sites. This chemical insertion is thus equivalent to a diffusion process. It may be associated with a phase transition/change of the solid that we do not consider explicitly in the present description, but which could be characterized by an empirical average diffusion coefficient.

In CV responses, physical and chemical insertion thus appear as charge storage processes associated with a capacitive current and a Faradaic current respectively, paralleling the distinction between capacitors and batteries. In this framework, it should be emphasized that the inserting ion may be involved in both the Faradaic process (insertion in the solid conductive material) and the capacitive process (in the formation of the double layer in mesopores and of a compact layer in nanopores). This mutual dependence of the capacitive and Faradaic processes makes a completely general description difficult and of little practical usefulness. It thus appears more productive to restrict analysis to the following simpler situations. One involves the presence in large excess of a "blocking supporting electrolyte",[11,12] whose ions are not able to chemically insert in the solid structure. Its role is thus to set up the double layer (or the compact layer in nanopores) at the bulk material/pores interface. A second, commonly encountered situation is when the inserting ion C^+ is in large concentration in the electrolyte so that its concentration at the solid material/pores interface can be considered to be constant and practically the same as that in the bulk of the solution. Within this framework, Figure 2 summarizes the various physicochemical events that require consideration, namely: electrolyte transport in solution, electrolyte transport in the mesopores, electron transport in the solid, solid/electrolyte interface charging, kinetics of electron coupled ion in/out process at the pores' solid/electrolyte interface, ion transport in the solid. Transport of the inserting ion in solution and in the pores is described as diffusional because the additional blocking electrolyte is responsible for Ohmic transport in both the solution and the pores. Differential capacitance at the solid material/electrolyte interface is assumed to be constant and also set by the blocking electrolyte. The following parameters therefore need to be introduced: resistance of the solution (R_{sol}), global resistance of the pores (R_P), total resistance of the solid conducting material (R_B), total differential capacitance (C_d) of the interface between the pore walls, and the conducting material. The main electrochemical event

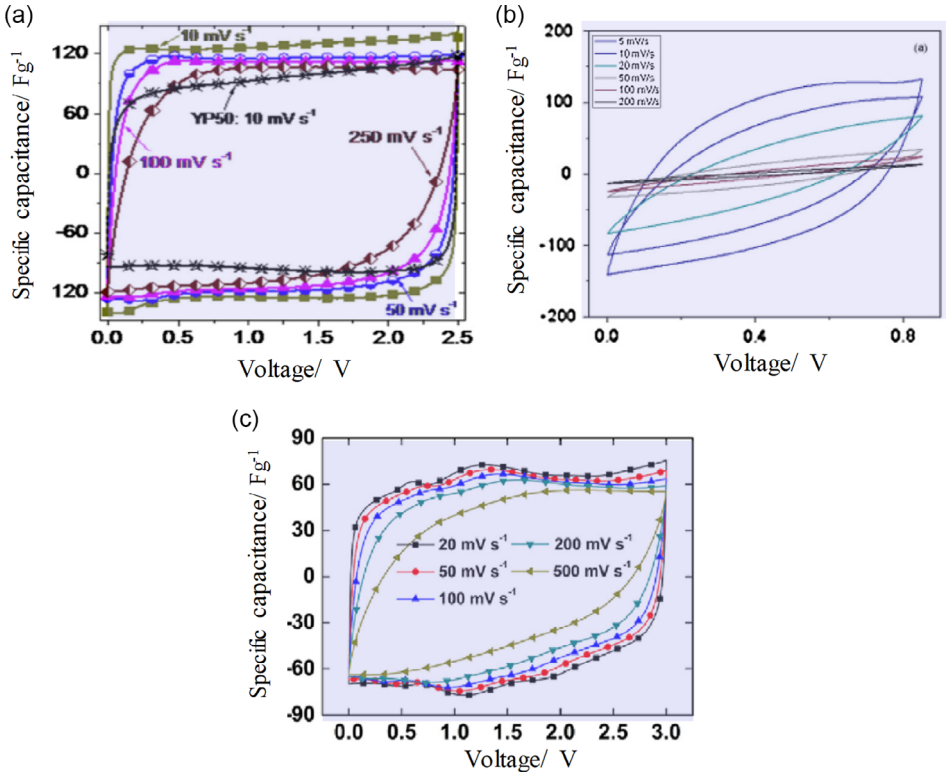

Figure 3. Examples of typical CV capacitive response of the three categories of porous electrode material. a) porous carbon electrode. Adapted with permission.[5] Copyright 2016, Elsevier. b) amorphous MnO_2 in the potential range of electronic conduction. Adapted with permission.[7] Copyright 2016, Elsevier. c) a MYxene electrode. Adapted with permission.[18] Copyright 2016, Elsevier. The capacitance plateaus reached at the ends of the potential scan reflect the proportionality of the current to the scan rate as expected for CV capacitive charging.[34] The preceding portion of the CV response reflects the effect of ohmic drop in the electrode and solution, whose increase parallels the increase in current resulting from raising the scan rate.

in the system is the interfacial cation insertion–coupled–electron transfer taking place at this interface. It is characterized, within a Butler–Volmer framework, by a standard potential, E^0, a standard rate constant, k_S and a transfer coefficient, α. Diffusion in the various parts of the system is characterized by a series of diffusion coefficients, namely, D_{sol}, and D_P for the inserting ion in the solution and in the pores, respectively. D_B is a diffusion coefficient pertaining to the solid electrode material, noting that the process is actually a series of ion self-exchange reactions between redox sites coupled with electron exchange with the electronic conductive structure, which is formally equivalent to a diffusion process.[13]

In the following sections, modeling of both capacitive and Faradaic processes is developed within the above framework and geometries of the porous electrode in which structural details have been simplified and averaged so as to get a minimal number of parameters governing the CV responses.

2.1. Capacitive Current

The capacitive current can be analyzed by means of a transmission line model (**Figure 4**).[14] The transient regime preceding the capacitance plateau is worth a close examination as it may be easily confused with a reflection of ion diffusion.[7] Under usual conditions of concentrations and scan rate, diffusion of the ions engaged in the double layer is in fact much too rapid to disturb its equilibrium status.[4,15,16]

The nanopores contribute to the overall capacitance but only through the charge imprisoned in compact double layers. Indeed, since the nanopores have a thickness comparable to the Debye screening length (λ_D), a classical double-layer structure cannot develop and the electrostatic potential in the nanopore space can be regarded as constant.[17] In the mesopores, the effect of ion diffusion may be neglected as in the case of planar electrodes. The capacitive CV responses are thus governed by potential Ohmic drop in the pores (and to a lesser extent in the solution), which can be analyzed according to the transmission line model represented in Figure 4a. The linear scan voltammogram response in Figure 4b is represented as a function of the dimensionless time variable t/t_f, where $t_f = R_f C_f$ is the time constant of the cell, R_f and $C_f = S_a \times C_d$ being the total resistance and total capacitance of the film respectively (S_a is the total porous electrode surface area and C_d the differential capacitance). As time elapses, the capacitive current tends asymptotically to $C_f \nu$, corresponding to the full charging of the capacitance. To reach this value, the charging curve in the present porous film case is clearly different from the charging of a planar electrode having the same time response (dotted black line), $i_c/(C_f \nu) = 1 - \exp -t/t_f$. What is particularly striking is the short-time behavior (red curve). It indeed obeys the following equation.

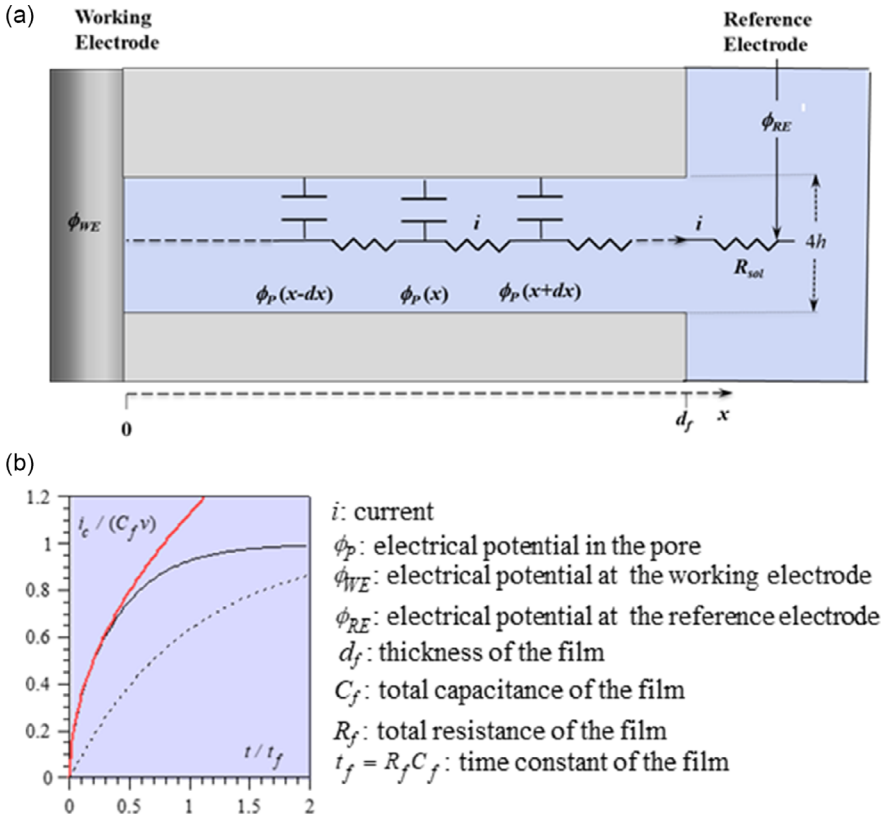

Figure 4. Schematic representation of a porous film. a) transmission line model. b) CV response (see text).

$$i_c/(C_f v) = (2/\sqrt{\pi}) \times \sqrt{t/t_f} \quad (1)$$

This is strongly reminiscent of a diffusion phenomenon. Indeed, the Galvani potential in each pore, $\phi_P(x)$, does obey the same Fick's law.

$$\frac{\partial \phi_P}{\partial t} = \frac{{d_f}^2}{R_f C_f} \frac{\partial^2 \phi_P}{\partial x^2} \quad (2)$$

as matter diffusion and also as heat transfer, even though these are phenomena of different physical nature. It should be particularly emphasized that, in spite of a formal resemblance, it has nothing to do with the diffusion of ions toward diffuse double layers that has been evoked and dismissed earlier.[4]

Figure 5a illustrates how increasing the scan rate makes it more difficult for the full charging of the capacitance and provides a description of the kinetics of charging. Another way of representing this effect consists of plotting the charged capacitance relative to the maximal capacitance against the scan rate, as shown in Figure 5b. This analysis has been applied to rationalize experimental data corresponding to capacitive charge storage in porous carbon,[4] as well as in MnO_2 electrodes which were first analyzed by means of the "pseudocapacitance" notion,[7] before it has been shown that they can be treated as real capacitances.[4]

Ohmic drop in the solution (through the resistance named R_{Sol} in Figure 2 and 4a) may add to the Ohmic drop in the porous structure that we just analyzed. This is an issue that has been discussed in detail in the past in the case of standard nonporous electrodes.[18,19] It may be either taken into account as a part of processing the data or compensated by electronic devices such as those based on positive feedback. The same strategies may be applied in the present case taking into account the specific characteristics of porous electrode[14] or the precaution that it should not interfere in the part of the CV response that is relevant to the porous structure.[20]

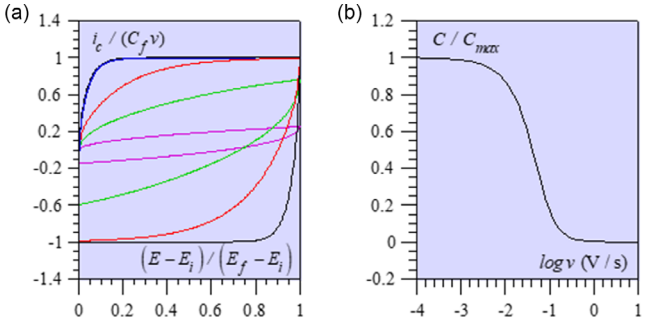

Figure 5. Charging characteristics of porous films. a) Dimensionless CV responses as a function of the adimensionalized scan rate, $R_f C_f v/(E_f - E_i) = 0.1$ (blue), 0.5 (red), 2 (green), 20 (magenta) (v: scan rate, E_i, E_f: initial and inversion values of the cyclic potential scan). b) Charged capacitance versus the maximal capacitance as a function of the scan rate.

2.2. Faradaic Current

The Faradaic current (i_f) corresponds to localization of electrons at specific sites in the bulk electrode material, associated with cation insertion, which thus maintains electroneutrality and allows current flowing through the cell. Cation insertion occurs at the solid/electrolyte interface through the potential difference between the two phases. In sake of simplicity, the Faradaic event is assumed to take place within a potential range where the bulk material is electronically conductive and where the capacitive current has reached the steady value, $C_f v$. It is then considered that the ohmic drop in the solution may be considered as negligible in view of the large concentrations of the blocking electrolyte or of the inserting ions.

From **Figure 6**, it is seen that, the underlying electrode having a surface area, $S = L \times H$, the apparent solid/electrolyte interface surface area is $S_a \approx HL2d_f/(2d_i + 4h)$ (the electrode is assumed to be large and porous enough so that the edge surface area can be neglected). As sketched in Figure 6, the inserting cation, C^+, diffuses in solution (in a linear semi-infinite way) with a diffusion coefficient D_{sol}, and in the pores (in a linear finite way) with a diffusion coefficient D_P. We thus do not consider lateral diffusion in the pores as well as no pore entrance diffusional effect. Refinements including such effects should follow the developments in ref. [21].

A homogeneous distribution of immobile redox centers (volumic concentration C^B) is assumed within the solid material. Hence chemical insertion of C^+ in the material structure occurs at the material/electrolyte interface through an ion-coupled electron transfer process between three partners: an oxidized form (Ox) of the immobile redox centers at the interface, an electron, free to move in the conductive material, and the cation C^+ in the pore so as to finally produce a reduced species Red, in which the C moiety allowing to localize the electron on the redox site has been integrated.

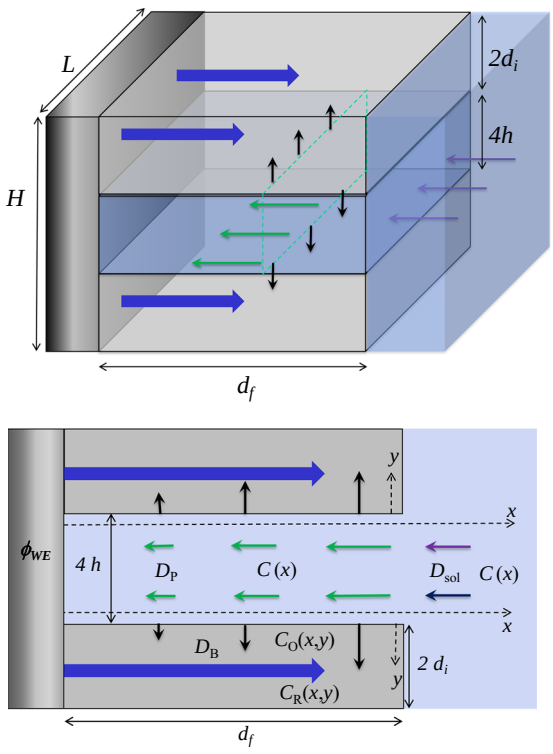

Figure 6. Sketch of porous electrode modeling (see text).

$$C^+_{\text{pore}} + e^- + \text{Ox} \rightleftarrows \text{Red} \tag{3}$$

The insertion kinetics is described by a Butler–Volmer-type equation characterized by a standard rate constant k_S, a standard potential E^0, and a transfer coefficient α assumed to be equal to 0.5. The electrode potential at the position x where C^+ inserts into the structure is $E(x) = \phi_B(x) - \phi_P(x)$ where $\phi_B(x)$ and $\phi_P(x)$ are the Galvani potential of the material structure and the pores respectively.

In order to account for possible nonideal behaviors of redox insertion sites such as interactions between redox centers or distribution of local environment, we introduce activity coefficients for the oxidized and reduced sites at the interface as previously described.[8] Ion transport within the bulk film is assumed to occur through a series of self-exchange ion-coupled electron transfers equivalent to a diffusion process with a diffusion coefficient D_B (note that the Galvani potential in the material structure is assumed to be uniform at a given x position, i.e., it does not depend on y; hence there is no migration term for C^+ in the material structure. We also assume that there is no hopping, hence no diffusion, of C^+ along the x axis). The present description does not explicitly consider phase transition in the solid material[22] but the apparent diffusion coefficient D_B can be considered as an ad hoc parameter associating several phenomena.

We focus the analysis on the case where the resistance of the solution can be neglected owing to the large concentration of blocking electrolyte or inserting ions in the solution. Nevertheless, the CV Faradaic current potential responses $i_f(E)$ depend on a considerable number of experimental intrinsic and operational parameters. The goal of the analysis is the derivation of the CV responses that are predicted to be observed for any set of values of all experimental intrinsic and operational parameters. Comparison between the predicted and observed CV responses, or at least remarkable features, such as peak currents and potentials, is the source from which the reaction mechanism can be ascertained and characterized thermodynamically and kinetically, as well as the dimensionless expression of the current and the potential scales of the CV responses. Concerning the latter point, the current, i_f, will be expressed in three different manners according to the context. The first of them refers to the diffusion of the inserting ion in the solution.

$$\psi_{f,sol} = \frac{i_f}{FSC^{Sol}_{C^+}\sqrt{\frac{Fv}{RT}D_{sol}}} \tag{4}$$

(v: scan rate, S: geometric surface area of the base electrode, $C^{Sol}_{C^+}$: concentration of the inserting ion in the bulk of the solution, diffusion coefficient of the inserting ion in the solution). The second matches the diffusion-like ion-coupled electron hopping between redox sites in the electrode material.

$$\psi_{f,B} = \frac{i_f}{FS_aC^B\sqrt{\frac{Fv}{RT}D_B}} \tag{5}$$

(S_a: surface area of the interface between the pores and the electrode material. base electrode, C^B: total concentration of the redox centers in the bulk of the electrode material, D_B: coefficient of the diffusion-equivalent ion-coupled electron hopping, in the electrode material). The third aims comparison with responses of the surface-wave type.

$$\varphi_f = \frac{i_f}{FS_a d_i C^B \frac{Fv}{RT}} \tag{6}$$

(d_i: half-thickness of the electrode material, see Figure 6).

The potential scale is conveniently expressed as.

$$\xi = -\frac{F}{RT}(E - E^0) + \ln(C^{sol}_{C^+}/C^0) \tag{7}$$

($E = \phi_{WE} - \phi_{RE}$, E^0: standard potential of the $Ox + C^+$/Red couple). In view of the large number of intrinsic and operational parameters governing the CV responses, it is worth bestowing also a dimensionless formulation of the problem to reduce the number of actual parameters to a minimum. The following expressions of these various dimensionless parameters derive from the mathematical analysis of the set of equations and conditions that govern the physical chemistry at work as detailed in the Supporting Information (SI) first section. A minimal set of ten dimensionless governing parameters is required in this purpose. They may be selected as done below, albeit they could be replaced by any combination of these items provided a new set of ten independent dimensionless parameters are generated.

$$\begin{aligned}
&\sigma = \frac{d_i + 2h}{4h},\ \delta_{sol} = \frac{D_{sol}}{D_P},\ l_P = \frac{d_f}{\sqrt{D_P RT/Fv}},\\
&l_B = \frac{d_i}{\sqrt{D_B RT/Fv}}, \gamma = \frac{S_a}{S}\frac{C^B}{C^{sol}_{C^+}}\sqrt{\frac{D_B}{D_{sol}}} = \frac{d_f}{d_i + 2h}\frac{C^B}{C^{sol}_{C^+}}\sqrt{\frac{D_B}{D_{sol}}},\\
&\Lambda = \frac{k_S}{\sqrt{D_B Fv/RT}}\left(\frac{C^{sol}_{C^+}}{C^0}\right)^{1-\alpha}\alpha,\ \rho_P = r_P\frac{F^2}{RT}\sqrt{D_P D_{sol}}C^{Sol}_{C^+},\\
&\rho_B = r_B\frac{F^2}{RT}\sqrt{D_P D_{sol}}C^{Sol}_{C^+},\ g
\end{aligned} \tag{8}$$

(with $S_a/S \approx d_f/(d_i + 2h)$).

We note that σ is a geometrical factor that compares the dimensions of the pores and of the electrode material. δ_{sol} relates the diffusion coefficients of the inserting ion in the solution and in the pores. Diffusions in the pores and equivalent "diffusion" in the bulk material, in the x and y directions, respectively, are governed by the two parameters l_P and l_B, which measure the ratio between the dimensions of the pores, deepness and width, and the lengths characterizing the diffusion or equivalent diffusion layers in the pores and in the electrode material respectively. γ is a mixed parameter that involves the ratio of the surface area of the interface between the pores and the electrode material and of the base electrode, the ratio of the total concentrations of the redox couple in the electrode material and of the inserting ion in the bulk of the solution, as well as the ratio of the diffusion coefficients of these two species in the electrode material and bulk of the solution respectively. The kinetics of reaction appears through the parameters Λ and α. Ohmic drop in the pores and in the electrode material gives rise to the parameters ρ_P and ρ_B, respectively. Finally, g, which measures the interactions between the inserting ions, governs the slimming and fattening to the surface-type CV responses according to a Frumkin-type isotherm.

We now successively discuss three limiting situations of most practical interest.

2.2.1. Shallow Pores. Fast Transport in Pores

These limiting situations are achieved as soon as $l_P = d_f/\sqrt{D_P RT/Fv} \to 0$. To help focusing on the role played in these conditions by transport through the electrode material and the reaction taking place at the pore/ electrode material interface, we assume that Ohmic drop is negligible ($\rho_P \to 0$ and $\rho_B \to 0$) and that, owing to the large concentration of inserting ion in solution, $\gamma \to 0$ as well as fast transport in solution: $\delta_{sol} \to \infty$. Lateral interactions are also neglected ($g = 0$) in a first stage, before being specifically addressed. Under these conditions, the problem may be readily treated by means of close-form expressions (see Supporting Information), similarly to previous analysis of proton insertion in a planar electrode.[23] The system is governed by two parameters l_B and Λ. As sketched in **Figure 7**a, the ensuing zone diagram delineates four limiting zones with peak currents being either proportional to $\sqrt{v}$ or to v depending on whether insertion in the electrode material is diffusion limited ($l_B \to \infty$) or governed by the interfacial reaction ($l_B \to 0$). The four limiting zones are those in which the CV response does not dependent on any parameter.

Their acronyms were selected to recall the nature of the responses (S for surface wave, D_{in} for ion-coupled electron hopping equivalent diffusion inside the solid electrode material, the superscript r or irr indicating the total reversibility of irreversibility of the interfacial reaction, respectively). The boundaries between zones are based on a 5% relative uncertainty on peak currents in favor of the limiting behavior.

Changing the scan rate amounts to move the system along $\Lambda \times l_B = (d_i k_S/D_B)(C^{Sol}_{C^+}/C^0)^{1-\alpha} = \text{cst}$ straight lines (in red) in the zone diagram. Figure 7b shows typical CVs and Figure 7c, the corresponding variation of the peak current as a function of: $\frac{l_B}{\Lambda} = \frac{d_i F/RT}{k_S (C^{Sol}_{C^+}/C^0)^{1-\alpha}}v$. The constancy of $\psi^p_{f,sol}$ for large values of the latter parameter indicates that the peak current is proportional to $\sqrt{v}$ in this range, thus matching a diffusion control of the current-potential response. As the parameter decreases, the response tends asymptotically toward the characteristics of a surface reaction. This is in particular the trend expected upon lowering the scan rate, while keeping constant the other ingredients of the parameter l_B/Λ.

Lateral interactions induce broadening ($g > 0$) or slimming ($g < 0$) of the CV responses but do not significantly modify the broad evolution of the peak current with scan rate (see Figure S1, Supporting Information).

Several examples can be found in the literature where the limiting cases described above can be identified, at least approximately. Porous transition metal oxides inserting Li^+ upon reduction are probably the most studied porous electrodes as they are components of Li-ion batteries.[24] Experiments are usually performed in the presence of a large concentration of

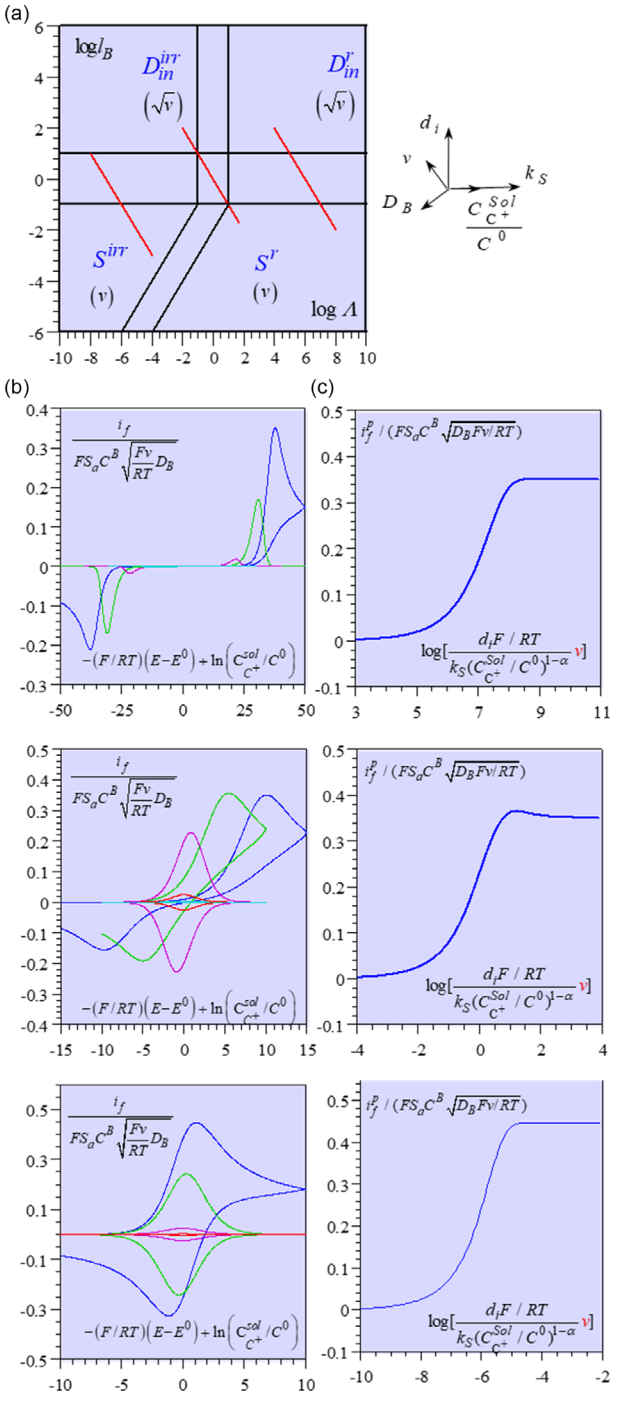

Figure 7. a) Schematic zone diagram for $\rho_P \to 0$, $\rho_B \to 0$, $\gamma \to 0$, $\delta_{sol} \to \infty$, $l_P \to 0$, and $g = 0$ with, for the four limiting zones (S^r, D_{in}^r, S^{irr}, D_{in}^{irr}), indication of the proportionality of the peak current to either v or $\sqrt{v}$. Red lines correspond to $\log(\Lambda \times l_B) = -7$, 0, 6. b) Dimensionless CV responses for (from top to bottom): $\log\left[\frac{d_i k_S}{D_B} C_{C^+}^{Sol}/C^0)^{1-\alpha}\right] = -7$ and $1 \le \log\left[\frac{d_i F/RT}{k_S (C_{C^+}^{Sol}/C^0)^{1-\alpha}} \nu\right] \le 9$, $\log\left[\frac{d_i k_S}{D_B} C_{C^+}^{Sol}/C^0)^{1-\alpha}\right] = 0$ and $-4 \le \log\left[\frac{d_i F/RT}{k_S (C_{C^+}^{Sol}/C^0)^{1-\alpha}} \nu\right] \le 4$, $\log\left[\frac{d_i k_S}{D_B} C_{C^+}^{Sol}/C^0)^{1-\alpha}\right] = 6$ and $-10 \le \log\left[\frac{d_i F/RT}{k_S (C_{C^+}^{Sol}/C^0)^{1-\alpha}} \nu\right] \le -2$ c) Variation of the dimensionless peak current with the parameter $l_B/\Lambda = \frac{d_i F/RT}{k_S (C_{C^+}^{S}/C^0)^{1-\alpha}} \nu$ for log $(\Lambda \times l_B) = -7$, 0, 6 (from top to bottom).

electrolyte (typically 1 M) so that not only Ohmic drops in the solution and electrode are small as already discussed but also the diffusion in solution can be neglected. A typical example representative of a transition between surface wave (S^r zone) and diffusion-like transport in the inserting material (D_{in}^r zone) can be found in another study[25] where insertion/extraction of Li^+ in $LiFePO_4$ was investigated. The CV response is diffusion controlled when $\nu > 10$ mV s^{-1} with interference of both electron transfer kinetics (increase of peak separation) and probably some Ohmic drop as well. Transition to a surface wave is observed as ν is decreased below 10 mV s^{-1}. Similar results have been reported for $Li_{1-x}CoO_2$ material in which case electron transfer kinetics at the material–electrolyte interface was well described by a Butler–Volmer kinetics together with an interaction parameter $g = -4.2$.[26] A similar value was found for Li^+ insertion/extraction from $Li_4Ti_5O_{12}$.[27] Ion-coupled electron transfer kinetics has been scrutinized in detail in the case of carbon-coated $LiFePO_4$ and it appears that the driving force-activation law follows Marcus–Hush–Chidsey model rather than the simplified linearized Butler–Volmer law which remains valid over a small driving force variation range.[28]

Very different CV shapes can be observed depending on the amorphous or crystalline nature of the inserting material as exemplified on $LiFePO_4$/graphitic carbon electrodes.[29] Crystalline domains lead to thin peaks with a transition (at 0.1 V s^{-1}) between a surface wave at low scan rate and a diffusion-controlled wave at high scan rate. Amorphous domain leads to a broad surface wave over the full range of scan rate indicating a faster Li^+ apparent diffusion and very different lateral interactions at the material entrance. Li^+ insertion in other oxide such as TiO_2 was also studied using CV.[30] At large enough Li^+ concentration in the electrolyte, insertion was shown to be controlled by Li^+ diffusion with interference of ioncoupled interfacial charge transfer. For thick films, the insertion process was additionally limited by Ohmic drop in the electrode material.

2.2.2. Fast Insertion in Solid Electrode Material. Transport in the Pores

We now turn to the situation where transport in the pores interferes. In order to put the focus on this effect, we still consider the case of a system where ohmic drop is negligible ($\rho_P \to 0$ and $\rho_B \to 0$) with a fast transport in solution ($\delta_{sol} \to \infty$). It is also assumed that the electrode material thickness is relatively small and/or that transport through it is fast, corresponding overall to $l_B \to 0$. For each x, insertion of ions in the electrode material along the y coordinate thus populates a fraction θ_{Red} and $\theta_{Ox} = 1 - \theta_{Red}$ of the reduced and oxidized forms of the Ox/Red couple in the electrode material, respectively. The dimensionless CV responses are then best expressed as

$$\varphi_f(\xi) = \frac{i_f}{FS_a d_i C^B} \frac{RT}{Fv} \tag{9}$$

They are fully governed by four dimensionless parameters, namely, $l_P = \frac{d_f}{\sqrt{D_P RT/Fv}}$, $\frac{\Lambda}{l_B} = \frac{k_S}{d_i Fv/RT} \left(\frac{C_{C^+}^{sol}}{C^0}\right)^{1-\alpha}$, $\Xi_B = \frac{l_B}{l_P} \gamma\sigma \sqrt{\delta_{sol}} = \frac{d_i}{4h} \frac{C^B}{C_{C^+}^{Sol}}$, and g (see SI).

Ξ_B represents the global charge storage capability of the electrode solid material, whereas Λ/l_B relates to the charge storage rate. The system is then equivalent to sequestration in 1D pores as previously described.[21]

The case of large storage rates ($\Lambda/l_B \to \infty$), meaning that reaction (1) is at equilibrium at the pores/ electrode solid material interface, is particularly worth addressing since it offers good view on the effect of transport in the pores. If interactions between inserted ions ($g = 0$) are additionally neglected, the dimensionless CV responses $\varphi_f(\xi)$ depend upon the two dimensionless parameters l_P and Ξ_B characterizing transport in the pore and global charge storage capability of the electrode material, respectively. In these conditions, the zone diagram in **Figure 8**a helps navigating between the various limiting situations that can be encountered according to the values of the intrinsic and operational parameters.

When $l_P \to \infty$, meaning that the pores are deep or that, for this reason or any other, transport of the inserting ions in the pores is slow, the CV responses are a function of the single parameter Ξ_B and may be expressed by (see SI)

$$\varphi_f = \frac{1}{\Xi_B}\left(-1 + \frac{[\Xi_B + 1 + \exp(-\xi)]}{\sqrt{[\Xi_B + 1 + \exp(-\xi)]^2 - 4\Xi_B}}\right)\frac{\exp(-\xi)}{2} \qquad (10)$$

Two limiting subcases are reached for $\Xi_B \to \infty$ and $\Xi_B \to 0$, as represented in Figure 8b,e, respectively (although the CV responses have the same surface wave shape in both cases, they differ both in current height and potential scale). They are noted S^r and S^r_{pore} respectively in the zone diagram. They are typical of the simplest behaviors of the system in the sense that its characteristics do not depend then on any parameter. Surface waves are obtained, corresponding to saturation of the charge storage capacity by the large amount of ions present in the pores ($\Xi_B \to 0$) or, alternatively to storage of all ions present in the pores ($\Xi_B \to \infty$) but without replenishment from the solution due to the very slow transport of ions in the pores ($l_P \to \infty$). Another zone in which the CV responses do not depend on any dimensionless parameter value, noted D^r_{pore} in the diagram, corresponds to both $\Xi_B \to \infty$ and $l_P \to 0$, with $\sqrt{\Xi_B}/l_P \to \infty$ (the converse condition brings back the system to the standard surface wave response that belongs to an extremely extended zone of the diagram). This D^r_{pore} response is shown in Figure 8c (see SI for numerical computation). Since $\Xi_B \to \infty$, the relatively small number of ions initially present in the pores is quickly inserted during the forward scan. The ions then replenish the pores via diffusion from the solution leading to the appearance of a diffusion-type wave. On the reverse scan, the ions are deinserted from the bulk material, leading to a desorption type-wave shape.

Figure 8d features what happens in a one-parameter depending zone (noted *d* in the diagram) of particular interest since it makes it clearly appear that the current is made of two potential-separated contributions involving a surface-wave and a diffusion-controlled contribution. The ratio of the two contributions is governed by the magnitude of the parameter $l_P/\sqrt{\Xi_B} = d_f\sqrt{(4h/d_i)(C^{Sol}_{C^+}/C^B)/(D_P RT/Fv)}$ as fully illustrated in the details of Figure 8d. The first of these is a surface type wave corresponding to insertion of ions initially present in the pores. It becomes the only one as $l_P/\sqrt{\Xi_B} \to \infty$. The second contribution corresponds to insertion of ions replenishing the pores from solution *via* diffusion. It is therefore a diffusion-type wave, which becomes predominant as $l_P/\sqrt{\Xi_B} \to 0$, leading back to the D^r_{pore} response. Similar observations may be made on Figure 8e–g.

Still another view on the effect of pore diffusion is gained when the system representative point in the zone diagram is moved along one of three red horizontal segments in Figure 8a, from log $l_P = 0$ to 1.5, from three increasing values of Ξ_B, 0.1, 1, 10. The resulting dimensionless CV responses are displayed successively in Figure 8h–j. While the first of these values of Ξ_B is clearly too small to foster any significant deviation from the fast-pore-diffusion/surface wave behavior, with the two next values, the system enters zones in which the competition between the two behaviors definitely shows up, as shown in the detail of Figure 8i,j. The variations of the corresponding peak currents are summarized in Figure 8k for the same three values of Ξ_B. This was also the occasion to examine more closely the C^+ concentration profiles and the red-form fractional coverage profiles in one of these cases ($l_P = 31.2$ and $\Xi_B = 10$), as shown in Figure 8l,m for four values of the potential variable ξ along the forward scan. There is first a depletion of ions at the bottom of the pores with θ_{Red} remaining small because $\Xi_B \gg 1$. At the entrance of the pore, ions are then diffusing from the solution leading to an additional contribution to the current as these ions insert quickly in the bulk material up to saturation of the sites. This results in a step profile of θ_{Red} at the entrance of the pores. This ionic front then slowly progresses along the pore; with a linear concentration profile as already described in ref. [21].

2.2.3. Role of Diffusion in Solution. Contrasting the Effects of Diffusion in Solution and Diffusion-Like Ion-Coupled Electron Hopping in the Solid Electrode Material

So far, we have assumed that mass transport in solution is not interfering in the Faradaic response. This condition is achieved if $\delta_{sol} \to \infty$ in the two preceding limiting cases. It more generally applies if the inserting ion concentration is large in solution and if diffusion in pores is slowed down due to small size and tortuosity. However, to elucidate to which extent the electrolyte in the pores can be consumed, it might be useful to lower the inserting ion concentration in the solution (so as to increase the pore storage capability parameter Ξ_B).[30] In such a case, provided δ_{sol} is not very large, mass transport in solution may interfere. Decreasing the electrolyte concentration may also be useful to identify the actual provider of the inserting ion as it is the case for example with protons emanating from a buffer component[8,23,31] or from a water molecule in the solvation sphere of a multivalent cation rather than insertion of the cation itself.[32]

We simplify the analysis by considering again shallow pores and/or fast transport in the pores ($l_P \to 0$) and no significant Ohmic drop ($\rho_P \to 0$, $\rho_B \to 0$). If attention is additionally focused on fast interfacial reaction (1) ($\Lambda \to \infty$), the system is simply governed by two parameters l_B and γ (for the sake of simplicity, we also consider ideal behaviors, i.e., $g = 0$). As described elsewhere for the specific case of proton insertion from a buffer component (see SI for adaptation to ion insertion),[23] it is conveniently

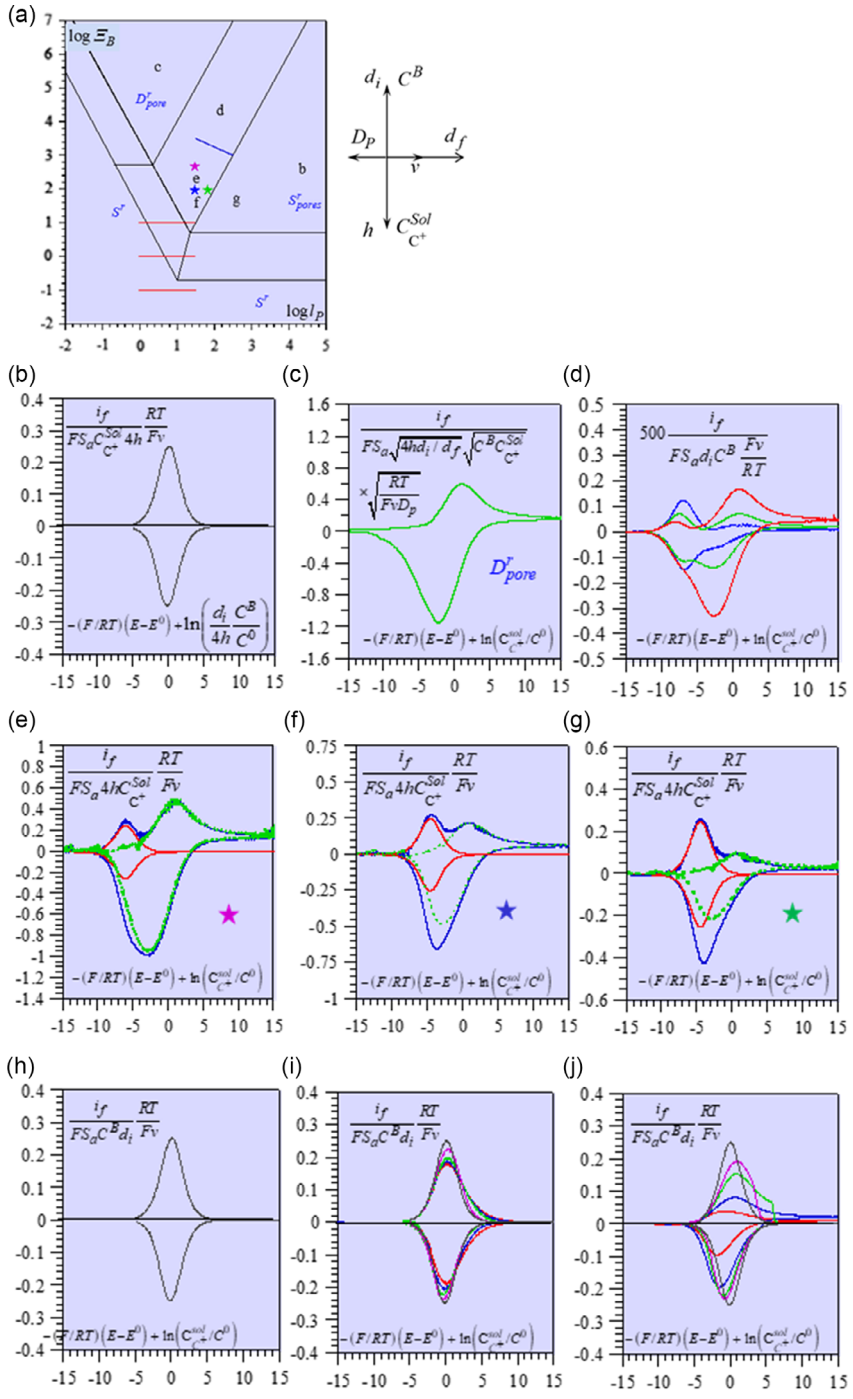

Figure 8. Fast insertion in solid electrode material ($l_B \to 0$, see text). a) Zone diagram showing the various subcases. b–d) typical dimensionless responses corresponding to the situations indicated by the corresponding letter on the zone diagram. In (d) $\log(l_P \Xi_B^2) = 8.5$ and $\log(l_P/\sqrt{\Xi_B}) = 1$ (blue), 0.375 (green), −0.25 (red); the representative point moves on the blue segment across the *d* zone. e,f,g) Dimensionless responses corresponding to the parameters indicated by stars in the zone diagram. Blue full CV, Red: surface type contribution, Dotted green: diffusion contribution obtained by subtraction of red CV from blue CV. h,i,j) Responses corresponding to the red segments in the zone diagram, for, successively h) $\Xi_B = 0.1$, i) 1, and j) 10 and, from bottom to top: $l_P = 0.936$ (grey), 2.5 (magenta), 6.24 (green), 12.5 (blue), 31.2 (red). k) variation of the dimensionless peak current with the scan rate through the parameter $d_f^2(F/RTD_P)\nu$ for, from top to bottom, $\Xi_B = 0.1$, 1, 10. l) concentration profile of the inserting ion in pores and m) fractional coverage in the *R* form of the redox couple over the pore/electrode material interface for $l_P = 31.2$ and $\Xi_B = 10$ at a series of successive electrode potentials: −15 (red), −3.5 (blue), −0.7 (green), and 15 (magenta).

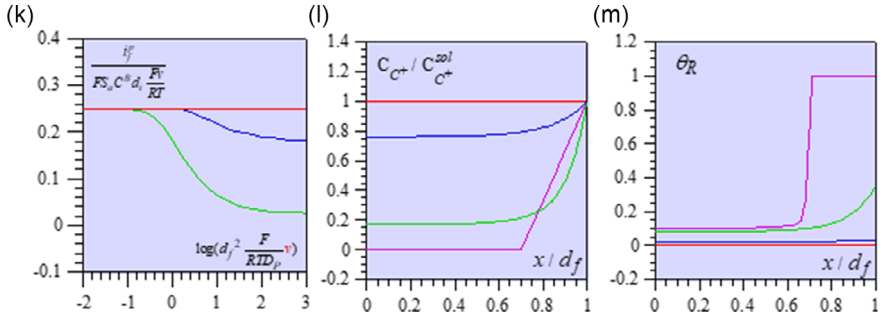

Figure 8. Continued.

represented by a 2D zone diagram (**Figure 9**) where the effect of scan rate corresponds to a vertical displacement.

In these systems, diffusion in the pores is fast and the only rate-limiting factors are diffusion of the inserting ions in the solution on the one hand and ion-coupled electron hopping in the solid electrode material, on the other. The CV responses expected in each of the zero-parameter zone are shown in Figure 9b, together with indication of proportionality of the peak current with the scan rate or square root of scan rate (see SI). Diffusion in solution is prevailing in the right-hand part of the diagram and vice versa for the left-hand part. The remarkable shape exhibited in the SD^r_{out} case features a classical diffusion control over the cathodic run followed by adsorptive anodic stripping on the reverse.[33] Alternatively, the left upper part of the diagram allows to extract the apparent diffusion coefficient of the inserting ion in the material as shown for Li^+ insertion in TiO_2 with $D^{Li^+}_{in} \approx 10^{-15}\ cm^2\ s^{-1}$.[33]

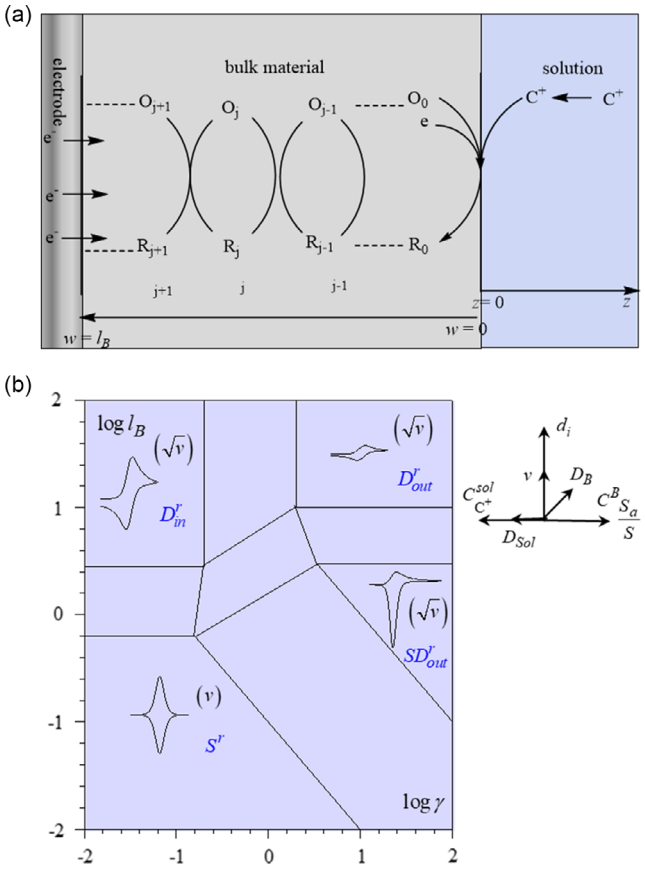

Figure 9. Effect of diffusion of the inserting ion in solution and of the diffusion-like ion-coupled electron hopping in the solid electrode material ($\rho_P \to 0$, $\rho_B \to 0$, $l_P \to 0$, $\Lambda \to \infty$, and $g = 0$). a) Scheme of diffusion in solution (right) and ion-coupled electron hopping in the solid electrode material (left). b) Zone diagram with indication of the proportionality of the peak current to either ν or $\sqrt{\nu}$ and CV responses in the zero-parameter zones.

3. Conclusion

The present contribution originated in the idea that CV of energy storage systems may offer a shortcut toward their analysis and optimization in real working conditions. This endeavor requires the assessment of the relationships linking the CV responses to the various intrinsic and operational parameters they depend upon. A first step in tackling the problem consisted in establishing the extended list of well-defined intrinsic and operational parameters that govern the CV responses. As their number is clearly very large a preliminary operation consists in formulating the problem in dimensionless terms. This consequently entails the grouping of the numerous intrinsic and operational parameters into a minimum set of dimensionless parameters, the variations of each of which representing collectively and precisely the variations of their ingredients. Even after this preliminary simplification and rationalization, the number of such necessary parameters remains much high to warrant the establishment of a general kinetic modeling of the CV responses that would cover all conceivable situations. A more pragmatic approach thus consists in singling out simpler situations of particular importance from a practical point of view. Along this view, a first distinction was made between physical and chemical ion insertion matching the occurrence of capacitive and Faradaic responses respectively. Concerning the latter issue, three main situations of practical interest were picked out and analyzed in details, namely the shallow pore limit, the thin solid material limit and the diffusion in the solution limit. The pertinence of this choice was illustrated by examples drawn from recent experimental reports. Two operational parameters play a major role in the functioning and diagnosis of these energy storage devices. One is the concentration of inserting ion in the solution. The other is the variation of the CV responses with the scan rate.

Supporting Information

Supporting Information is available from the Wiley Online Library or from the author.

Acknowledgements

This work was initiated together with Professor Jean-Michel Savéant, who passed on August 16, 2020. It is therefore dedicated to his memory. Partial financial support from the Agence Nationale de la Recherche (grant nos. Labex ARCANE, CBH-EUR-GS, and ANR-17-EURE-0003) is acknowledged.

Conflict of Interest

The author declares no conflict of interest.

Data Availability Statement

The data that support the findings of this study are available from the corresponding author upon reasonable request.

Keywords

cyclic voltammetry, energy storage, insertion, porous materials

Received: December 7, 2023
Revised: December 12, 2023
Published online: December 22, 2023

[1] a) W. Tiedemann, *ECS Trans.* **2008**, *16*, 23; b) R. B. Smith, M. Z. Bazant, *J. Electrochem. Soc.* **2017**, *164*, E3291; c) E. M. Ryan, P. P. Mukherjee, *Prog. Energy Combust. Sci.* **2019**, *71*, 118 Z. Chen, D. L. Danilov, R.-A. Eichel, P. H. L. Notten, *Adv. Energy Mater.* **2022**, *12*, 2201506.

[2] If the solid is not electronically conductive (as it is the case for example with lithium insertion material in lithium-ion batteries), an additional conductive material (carbon black) together with a binder (a polymer) is mixed with the divided solid to provide electronic conductivity.

[3] C. Costentin, T. R. Porter, J.-M. Savéant, *ACS Appl. Mater. Interfaces* **2019**, *11*, 28769.

[4] C. Costentin, J.-M. Savéant, *ACS Appl. Energy Mater.* **2019**, *2*, 4981.

[5] B. Dyatkin, O. Gogotsi, B. Malinovskiy, Y. Zozulya, P. Simon, Y. Gogotsi, *J. Power Sources* **2016**, *306*, 32.

[6] C. Costentin, D. G. Nocera, *J. Phys. Chem. C* **2019**, *123*, 1966.

[7] L. Coustan, P. Lannelongue, P. Arcidiacono, F. Favier, *Electrochim. Acta* **2016**, *206*, 479.

[8] C. Costentin, T. R. Porter, J.-M. Savéant, *ACS Appl. Mater. Interfaces* **2017**, *9*, 8649.

[9] C. Costentin, J.-M. Savéant, *Chem. Sci.* **2019**, *10*, 5656.

[10] M. Okubo, A. Sugahara, S. Kajiyama, A. Yamada, *Acc. Chem. Res.* **2018**, *51*, 591.

[11] J. Landesfeind, J. Hattendorff, A. Ehrl, W. A. Wall, H. A. Gasteiger, *J. Electrochem. Soc.* **2016**, *163*, A1373.

[12] J. Landesfeind, D. Pritzl, H. A. Gasteiger, *J. Electrochem. Soc.* **2017**, *164*, A1773.

[13] J.-M. Savéant, *J. Electroanal. Chem.* **1986**, *201*, 211.

[14] C. P. Andrieux, C. Costentin, C. Di Giovanni, J.-M. Savéant, C. Tard, *J. Phys. Chem. C* **2016**, *120*, 21263.

[15] H. Wang, L. Pilon, *Electrochim. Acta* **2012**, *64*, 130.

[16] L. Pilon, H. Wang, A. d'Entremont, *J. Electrochem. Soc.* **2015**, *162*, A5158.

[17] P. M. Biesheuvel, R. Zhao, S. Porada, A. van der Wal, *J. Colloid Interface Sci.* **2011**, *360*, 239.

[18] Z. Lin, D. Barbara, P.-L. Taberna, K. L. Van Aken, B. Anasori, Y. Gogotsi, P. Simon, *J. Power Sources* **2016**, *326*, 575.

[19] D. Garreau, J.-M. Savéant, *J. Electroanal. Chem.* **1972**, *35*, 309.

[20] a) A method named MUSCA (Multiple Potential Step Chronoamperometry) has been recently proposed to "reconstruct cyclic voltammograms with considerably lower ohmic drop contribution".[20b] Although illustrated by a MXene example, it is based on an approach only valid for standard non-structured electrodes. A further close evaluation this method in this framework[20c] showed that the cure is worse than the disease and opens the way to dangerous artefacts in data interpretation. Successive comments[20d] inconsistently attempt to save the method by evoking its application to structured electrodes in contradiction with its very principle; b) H. Shao, Z. Lin, K. Xu, P.-L. Taberna, P. Simon, *Energy Storage Mater.* **2019**, *18*, 456; c) C. Costentin, J.-M. Savéant, *Energy Storage Mater.* **2020**, *24*, 4; d) H. Shao, L. Zifeng, K. Xu, P.-L. Taberna, P. Simon, *Energy Storage Mater.* **2020**, *24*, 4.

[21] C. Amatore, *Chem. Eur. J.* **2008**, *14*, 5449.

[22] S. Y. Vassiliev, E. E. Levin, D. E. Presnov, V. A. Nikitina, *J. Electrochem. Soc.* **2019**, *166*, A829.

[23] Y.-S. Kim, V. Balland, B. Limoges, C. Costentin, *Phys. Chem. Chem. Phys.* **2017**, *19*, 17944.

[24] J. B. Goodenough, *Nat. Electron.* **2018**, *1*, 204.

[25] J. Come, P.-L. Taberna, S. Hamelet, C. Masquelier, P. Simon, *J. Electrochem. Soc.* **2011**, *158*, A1090.

[26] M. D. Levi, G. Salitra, B. Markovsky, H. Teller, D. Aurbach, U. Heide, L. Heiderb, *J. Electrochem. Soc.* **1999**, *146*, 1279.

[27] N. Oyama, S. Yamaguchi, Y. Mochizuki, T. Sarukawa, T. Shimomura, *Electrochemistry* **2010**, *78*, 375.

[28] P. Bai, M. Z. Bazant, *Nat. Commun.* **2014**, *5*, 3585.

[29] K. Kisu, E. Iwama, W. Naoi, P. Simon, K. Naoi, *Electrochem. Commun.* **2016**, *72*, 10.

[30] H. Lindström, S. Södergren, A. Solbrand, H. Rensmo, J. Hjelm, A. Hagfeldt, S.-E. Lindquist, *J. Phys. Chem. B* **1997**, *101*, 7717.

[31] Y. S. Kim, S. Kriegel, K. D. Harris, C. Costentin, B. Limoges, V. Balland, *J. Phys. Chem. C* **2017**, *121*, 10325.

[32] Y. S. Kim, K. D. Harris, B. Limoges, V. Balland, *Chem. Sci.* **2019**, *10*, 8752.

[33] R. H. Wopschall, I. Shain, *Anal. Chem.* **1967**, *39*, 1514.

[34] J.-M. Savéant, C. Costentin, *Elements of Molecular and Biomolecular Electrochemistry*, 2nd ed., Wiley, Hoboken, NJ **2019**.